RSC Advances

PAPER

View Article Online
View Journal | View Issue

Cite this: *RSC Adv.*, 2022, **12**, 9534

Preparation and properties of a novel poly(lactic-acid)-based thermoplastic vulcanizate from both experiments and simulations†

Xue Li,*[a] Hailan Kang,[b] Qiulan Luo[a] and Jianxiang Shen*[c]

A novel bio-based thermoplastic vulcanizate (TPV) material consisting of poly(lactic acid) (PLA) and a novel polymeric slide ring material (SeRM) was fabricated *via* isocyanate-induced dynamic vulcanization. The microscopic morphology, thermal properties, biocompatibility, and mechanical properties of the SeRM/PLA TPV material were comprehensively investigated, in turn by transmission electron microscopy, differential scanning calorimetry, *in vitro* cytotoxicity test, electron tension machine, and molecular dynamics simulations. Phase inversion in TPV was observed during the dynamic vulcanization, and TEM images showed that SeRM particles that were dispersed in PLA continuous phase had an average diameter of 1–4 μm. Results also indicated that an optimum phase inversion morphology was obtained at the SeRM/PLA blending ratio of 70/30 w/w. Glass transition temperature of PLA was found to be slightly decreased, owing to the improvement in interface compatibility by chemically bonding the PCL side chains (of SeRM molecules) and PLA chains. The tensile strength and elongation at break of TPVs were approximately 14.7 MPa and 164%, respectively, at SeRM/PLA blending ratio of 70/30, owing to the unique sliding effect of SeRM molecules when subjected to deformations. Cytotoxicity test results proved that the bio-based TPVs were fully non-toxic to L929 cells. In such aspects we believe that the bio-based TPV can be a promising material in the biomedical applications as an alternative of traditional commodity plastics.

Received 14th January 2022
Accepted 20th March 2022

DOI: 10.1039/d2ra00286h

rsc.li/rsc-advances

1 Introduction

Thermoplastic vulcanizates (TPVs) combine the rubbery elasticity and the thermoplastic properties. With the rapid development of TPVs over decades, they have been widely applied in many fields such as motor vehicles, buildings, electronics, biology, medicine, and so on.[1–5] In principal, a typical TPV consists of two main components, *i.e.*, a thermoplastic polymer as the continuous phase and a crosslinked elastomer as the dispersed phase.[6] TPVs are commonly prepared by the well-established dynamic vulcanization method, where the elastomer will be simultaneously crosslinked during its melt-mixing with the molten thermoplastic.[7–9] Specifically, the elastomer component, as a great majority of TPVs, will be broken up into smaller pieces with the increase of viscosity and elasticity through crosslinking, resulting in a transition from the initial continuous phase to the dispersed phase in the heterogenous blends. Such a phase inversion brings about the thermoplasticity to TPVs, which therefore can be processed by classical processing methods for plastic polymer materials and can as well be recycled and reclaimed. Additionally, the trimmings of TPVs during the processing can be reused by melt processing like the thermoplastics.

Although the TPVs have dual advantages of rubbery and plastic polymer materials, most of the two components (*i.e.*, rubber and thermoplastic) constructing TPVs are currently derived from petroleum resources, which consequently restricts the sustainable development of TPV industry. For example, the most widely-used TPVs are composed of ethylene propylene rubber (EPR) (or ethylene propylene diene monomer, EPDM) and polypropylene (PP),[10] and have a wide range of applications in the automotive industry, such as the closed systems, the interior trim, the car bases, and the electrical parts.[11,12] However, these two polymers are both obtained from petroleum resources and also cannot be degraded by simple methods, producing a huge pollution to environment. Therefore, to develop a fully bio-based TPV is of great significance to reducing the usage of limited petroleum resources and minimizing the damage to environment.[13]

Bio-based polymers can be, to a certain extent, good substitutes for conventional petroleum-based polymers. Currently,

[a]*Institute of Novel Materials, Jiaxing Nanhu University, Jiaxing 314001, P.R. China. E-mail: lixue_zjxu@163.com*

[b]*College of Materials Science and Engineering, Shenyang University of Chemical Technology, Shenyang 110142, China*

[c]*Department of Polymer Science and Technology, Jiaxing University, Jiaxing 314001, China. E-mail: shenjx@zjxu.edu.cn*

† Electronic supplementary information (ESI) available. See DOI: 10.1039/d2ra00286h

popular bio-based polymers are mostly starch-based, cellulosic-based and soy-based. One promising thermoplastic polymer among them is polylactic acid (PLA), which is obtained from some renewable resources such as corn and potato using a series of fermentation and chemical synthesis.[14–16] PLA has excellent mechanical properties and also ready biodegradability and good biocompatibility, which are widely applied in biomedical and other related fields apart from being used as traditional general-purposed plastics.[17–19] To this end, in this paper we choose the PLA as thermoplastic component of TPV, with the purpose of a potential biomedical application.

To prepare a bio-based TPV, the elastomer component should in principle be renewable and biocompatible. For example, Bueno-Ferrer *et al.* developed a bio-based thermoplastic polyurethanes (TPU) using diphenylmethane diisocyanate, 1,4-butanediol, and a polyol coming from a di-functional dimerfatty acid.[20] Liu *et al.* fabricated a bio-based and super-tough TPV consisting of PLA and a bio-based unsaturated aliphatic polyester elastomer (UPE).[21] Besides, Kang *et al.* prepared a non-toxic bio-based TPV by using PLA and a bio-based elastomer synthesized from bio-based diols and diacids, and the obtained TPV showed a tensile permanent deformation of less than 30% and also good reprocessability for recycling.[22] In the present paper, a novel bio-based elastomer, *i.e.*, slide ring polymer material (SeRM) is employed as the elastomer component of TPV. SeRM with supramolecular structure is a typical bio-based polymer and has novel structures that can be used as rubber components of bio-based TPVs. A plausible reason for us to choose SeRM is the pulley effect in SeRM[23] which is favorable to distributing stress and thus is expected to enhance the TPV elasticity.

2 Materials and methods

2.1 Raw materials

The polylactic acid (PLA) was purchased from Natureworks (USA) as grade 4032D. It has a density of 1.24 g cm^{-3}, a glass transition temperature of ~57 °C, a melting point of ~155 °C, and a melt flow rate (MFR) of 7 g/10 min at 210 °C. Slide ring polymer material (SeRM) was synthesized by following a procedure described in our previous publication,[23] and the commercial product can be bought from Tianjin Weirui Supramolecular Technology Co., Ltd, CAS number: 928045-45-8 JPN. The hydroxypropylated polyrotaxane was purchased from Advanced Softmaterials, Inc. (Tokyo, Japan). The toluene-2,4-diisocyanate (TDI) was purchased from Huntsman Chemical Trading (Shanghai) Co.

2.2 Synthesis and structure of slide ring polymer

As shown in Fig. 1, the giant SeRM molecule is composed of axial chain polyethylene glycol (PEG) molecule, ring-like cyclodextrin (α-CD) molecules, crown ether molecules at the chain terminal ends, and short ε-caprolactone (ε-PCL) chains anchored to the α-CDs, and its molecular weight typically ranges from 350 000 to 450 000. SeRM is synthesized through chemical modification of hydroxypropylated poly(rolane) molecules. Firstly, the hydroxypropylated α-CD molecules were driven to self-assemble into linear PEG chains to form a rotaxane-like structure. After that the bulky capping agents, crown ether, were added to the molecules so as to prevent hydroxypropylated α-CD slide away, and thus the hydroxypropylated poly(rolane) molecules were obtained. In the current experiments, the molecular weight of PEG is ~ 35 000 and the α-CD inclusion rate is 80–90%. SeRM was then prepared by bulk ring-opening polymerization of ε-PCL, using the hydroxyl group on the hydroxypropylated α-CDs as initiator and stannous octoate $Sn(Oct)_2$ as catalyst. More detailed information about the synthesis of SeRM can be found in our previous publication,[23] or referred to the work of Prof. Ito.[24–27] Since the PCL branch chains are attached to the cyclic α-CD molecule and there are no chemical bonds between the cyclic α-CD molecule and the axial PEG molecule, the PCL molecules are able to slide freely with α-CDs along the PEG axial chain. In this respect, such a giant polymer can be called as slide ring material.

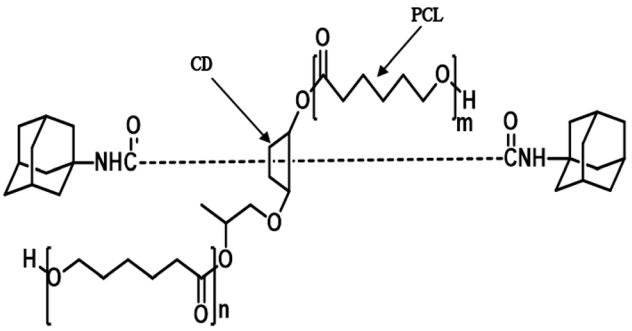

Fig. 1 Structural schematic of slide ring material (SeRM).

2.3 Preparation of bio-based TPVs

To begin with, SeRM and PLA were dried in a vacuum oven at 30 °C for 12 h and 60 °C for 24 h respectively before processing. SeRM/PLA TPV samples were then prepared by the following steps. (1) SeRM and PLA were blended by melt-mixing at a given blending ratio of SeRM/PLA (50/50, 60/40, 70/30, 80/20, respectively, by mass). The blending procedure was carried out in a Haake internal mixer (HAAKE Rheomix 600 OS, Thermal Fisher Scientific, USA) at 170 °C at a rotational speed of 80 rpm for 3 min. (2) The SeRM/PLA premix was continued to blend with the crosslinking agent, toluene-2,4-diisocyanate (TDI), for 12 min in the Haake internal (with the aforementioned condition unchanged); during such a mixing process, the SeRM/PLA sample was simultaneously and dynamically crosslinked. (3) The obtained samples were further molded into 1 mm thick sheet at 190 °C and 10 MPa pressure.

2.4 Characterization

Differential scanning calorimetry (DSC) was applied to collect the non-isothermal crystallization curves of SeRM/PLA TPVs. An atmosphere of nitrogen at 50 cm^3 min^{-1} was employed. After the specimens of 5–10 mg were placed in the crucible, the temperature was rapidly raised to 200 °C at a heating rate of

50°C min^{-1}, and kept at 200 °C for 5 min so as to eliminate the thermal history. The specimens were then lowered to −100 °C at a cooling rate of 10° min^{-1}, followed by heating them to 200 °C at 10°C min^{-1}. During the reheating process, the difference in heat flow rate (mW = mJ s^{-1}) between the specimens and inert reference as a function of temperature was recorded to examine the melting and crystallization behaviors of the TPVs.

The morphology was detected with an H-800-1 transmission electron microscope (TEM), Hitachi Co., Japan at 200 kV. The samples were cryomicrotomed at −100 °C to produce sections with 60 nm thickness, and then were vapor-stained with RuO_4 at room temperature for 20 min. Owing to the staining effect of the ether groups of PEG chains of SeRM molecules,[28] PLA would appear as the light domains and SeRM as the dark domains in TEM images.

The infrared spectra of absorption of TPVs were obtained by using Fourier transform infrared spectroscopy (FTIR), VERTEX 70v FT-IR spectrometer from Bruker, Germany. An attenuated total reflectance (ATR) method was employed. The scanning range was 4000–500 cm^{-1} with a resolution of 4 cm^{-1}.

The tensile mechanical properties of dumbbell-shaped specimens were measured in compliance with ASTM D638 specifications by using a CMT 4104 electrical tensile instrument (Shenzhen SANS Test Machine Co., Ltd, China) at a cross-head speed of 5 mm min^{-1} and room temperature. To obtain statistically significant data, five specimens at each group of SeRM/PLA TPVs were tested, and the data were thus collected and averaged.

In vitro evaluation of cytotoxicity of SeRM/PLA TPV materials was conducted following ISO 10993-5:199 standard, using L-929 mouse fibroblasts by MTT (tetrazolium salt 3-[4,5-dimethylthiazol-2-yl]-2,5-dipHnyltetrazolium bromide) assays. Each sample was sterilized with 75% ethanol, rinsed twice with PBS solution for 5 min each, and irradiated with Co^{60} source for 15 min. The samples were further incubated in Dulbecco's modified Eagle's medium (DMEM) at a proportion of 3 cm^2 mL^{-1} at 37 °C for 24 h. The obtained solution was subsequently filtered through pores of 0.22 μm to eliminate any indissoluble solid particles. L929 cells were cultivated in DMEM supplied with 10% fetal bovine serum (FBS) at 37 °C in humid 5% CO_2 condition at a density of 5.0×10^4 cells per well. After incubation, the initial cell medium was substituted by the previously prepared extract dilution, which allows the cells to proliferate for 3 days. A negative control group was set by without substitution (*i.e.*, still using the initial medium). MTT assay of 5 mg mL^{-1} was used to calculate the surviving fraction. After a 4 h incubation and a further aspiration of medium, blue formazan crystals were formed. The obtained crystals were then dissolved in isopropyl alcohol, and the absorbance at 570 nm was determined. Three independent tests were conducted to reduce the system error. The relative growth rate (RGR) was quantified as

$$\mathrm{RGR} = (A_{\mathrm{test}} - A_0)/(A_{\mathrm{control}} - A_0), \quad (1)$$

where A_{test}, A_{control}, and A_0 are the absorbance of samples, the controlled well containing cells with DMEM, and the solutions containing only DMEM, respectively.

2.5 Molecular dynamics simulation

Coarse-grained molecular dynamics simulations were performed to examine the mechanical properties of SeRM/PLA TPV materials. Polymers are represented by the canonical Kremer–Grest bead-spring model.[29] Each axial PEG chain and PLA matrix chain consists 100 beads of unit mass and diameter, connected by the a finite extensible nonlinear elastic (FENE) bonding potential,

$$E_{\mathrm{bond}} = -\frac{1}{2}K_{\mathrm{b}}R_0{}^2\ln\left[1 - \left(\frac{r_{ij}}{R_0}\right)^2\right], \quad (2)$$

where the spring constant $K_{\mathrm{b}} = 30.0\varepsilon/\sigma^2$, $R_0 = 1.5\sigma$, and r_{ij} is the bond length of two adjacent beads. Reduced units are employed in our simulations, and thus all calculated quantities are dimensionless. Here, ε, σ, and τ are the units of energy, length, and time, respectively. As depicted in Fig. 2a, at both ends of PEG chain are the crown ether molecules, which are modeled as relatively larger beads of diameter 2.0σ. α-CD molecules are modeled as hexatomic rings encircled around the axial chain. The aforementioned FENE potential is used to bond neighboring beads. To maintain their shape, a harmonic angle potential $E_\theta = K_\theta(\theta - \theta_0)^2$, with the spring coefficient equal $K_\theta = 100\varepsilon/\mathrm{rad}^2$ and the equilibrium angle equal $\theta_0 = 120^\circ$, and a harmonic dihedral potential $E_\phi = K_\phi(1 + \cos\phi)$ with $K_\phi = 100\varepsilon$, are imposed on the hexatomic rings. Each α-CD molecule are grafted with two short PCL chains (five-bead long), with one grafting site (or functional group) on the other end; the grafting site will be bonded to polymer matrix chains *via* the FENE potential during the equilibrium of simulation systems. To disentangle the pulley effect of slide rings on SeRM, our simulations are focused on the structural evolutions of SeRM molecules uniaxial deformation, and thus all polymer chains are set to fully flexible. Non-bonded interactions between all beads are described by a shift and truncated Lennard-Jones potential,

$$E_{ij}(r) = \begin{cases} 4\varepsilon_{ij}\left[\left(\frac{\sigma - \Delta}{r}\right)^{12} - \left(\frac{\sigma - \Delta}{r}\right)^{6}\right] - E(r_{\mathrm{c}}) & r < r_{\mathrm{c}} \\ 0 & r \geq r_{\mathrm{c}} \end{cases}, \quad (3)$$

where the energy well is set to $\varepsilon_{ij} = 1.0\varepsilon$, and the cutoff distance, for keeping the continuity of potential function, is set to $r_{\mathrm{c}} = 2.5\sigma$, in a unified manner. The shift distance Δ is determined by the radii of two interaction beads, $\Delta = r_1 + r_2 - \sigma$; for instance, $\Delta = 1.0\sigma$ for two capping agent beads of crown ether. Detailed information of the simulation model is given in Table 1. Previous simulation work[30] has demonstrated that such a coarse-grained model is adequate to mimic the static and dynamic characteristic behaviors of SeRM molecules.

All molecular dynamics simulations are performed in Large-scale Atomic/Molecular Massively Parallel Simulator (LAMMPS),[31] which are developed by Sandia National Laboratories. Starting from a simulated system at the desired melt density of $\rho^* = 0.85$, the canonical NVT ensemble at temperature $T = 1.0$ is employed to equilibrate the SeRM/PLA system, when the crosslinking between functional groups of PCL and PLA matrix chains are executed. Periodic boundary conditions

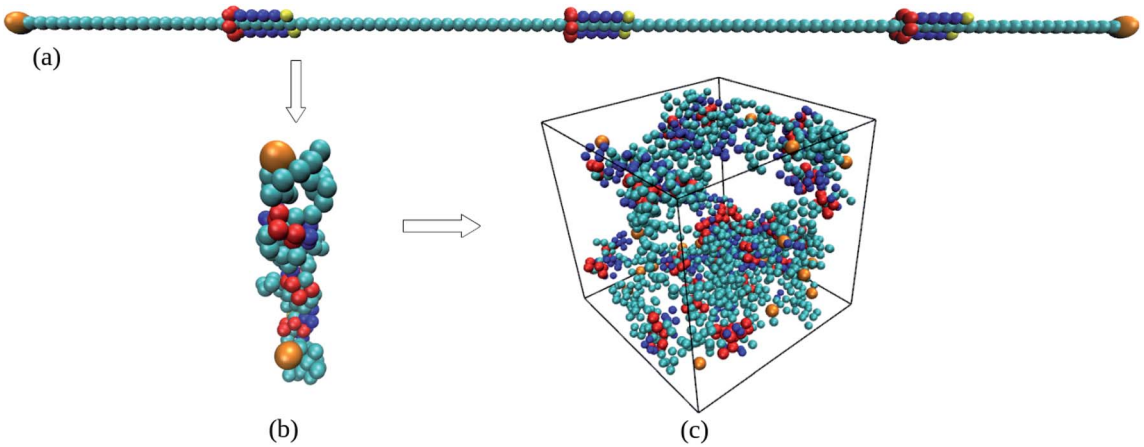

Fig. 2 Visualization of coarse-grained simulation models: (a) SeRM molecule, where cyan, red, blue, yellow, and orange spheres denote the axial PEG chain, cyclic α-CD molecules, PCL side chain except grafting sites (or functional group), grafting sites that will be bonded to polymer matrix chains, and the crown ether molecules as chain terminal ends, respectively. (b) VMD (Visual Molecular Dynamics) snapshot of SeRM molecule, in which the α-CD molecules are allowed to slide along the axial polymer, but are restricted to move slide away. (c) VMD snapshot of the whole simulation system, where the matrix chains are not displayed here for visual clarity.

are applied in all three dimensions. Velocity Verlet algorithm is adopted to compute Newton equations of motion and Nosé–Hoover thermostat to control the system temperature. The timestep is set to 0.001τ in all cases and the simulation reaches equilibrium after $\sim 2 \times 10^3$ τ. A VMD (Visual Molecular Dynamics) snapshot of the equilibrated system is displayed in Fig. 2c. To elucidate the mechanical performance of SeRM/PLA system, the uniaxial tensile deformation of simulation box is then carried out by using the SLLOD approach, where the box stretches along one direction (*e.g.*, z axial) at a strain rate of $0.0327\tau^{-1}$ and meanwhile shrinks in the other two directions to maintain a constant box volume. The average true stress in the elongation direction can be derived from the normal part of stress tensor, $(1+\mu)(-P_{zz}+P)$, where P_{zz} is the zz component of pressure tensor, P is the hydrostatic pressure, and μ is the Poisson's ratio. For such a uniaxial elongation deformation, incompressibility implies $\mu = 0.5$. More details about the simulations are available in our previous publications.[32–34]

3 Results and discussion

3.1 Dynamic vulcanization

Fig. 3 shows the mixing torque as a function of elapsed time for SeRM/PLA blends with varying blending ratio. After adding the SeRM/PLA blend into the mixer at ~2 min, the torque first increases dramatically and afterwards decreases slightly due to the softening and melting of the blend. The dynamic crosslinking process of SeRM/PLA blend starts from the addition of crosslinking agents TDI at ~5 min, when the mix torque is significantly elevated once again, reflecting a dramatic increase in both viscosity and elasticity of SeRM phase. Such a change can be ascribed to the chemical reactions between isocyanate groups of TDI molecules with the hydroxyl groups on PCL chains of (same or different) SeRM molecules, *viz.*, the crosslinks of SeRM. By the way, TDI molecules can also partially react with the terminal ends of PLA chains, resulting in the crosslinks between SeRM and PLA, which therefore facilitates the interface compatibility of the two components and thus the improves mechanical properties. While the reactive blending proceeds, SeRM particles are simultaneously destroyed into smaller ones under strong shear, therefore leading to the phase inversion, a prerequisite for fulfilling both rubbery elasticity and thermoplastics. The phase inversion will be discussed in the next section. The mixing torque eventually tends to be stable and changes slightly, and the torque after stabilization is seen to decrease with SeRM content increasing, mainly due to the much lower viscosity and stiffness of this rubber component. Indeed, the

Table 1 Bead Parameters in Simulation Model

Bead type	Representation	Bead diameter	Bead mass	Bead color in VMD snapshot (Fig. 2)
1	Cyclodextrin(α-CD)	1	1	Red
2	Grafting sites of PCL chains	1	1	Yellow
3	PCL chains (except grafting sites)	1	1	Blue
4	Crown ether	2	8	Orange
5	PEG chains	1	1	Cyan
6	PLA chains	1	1	Not shown

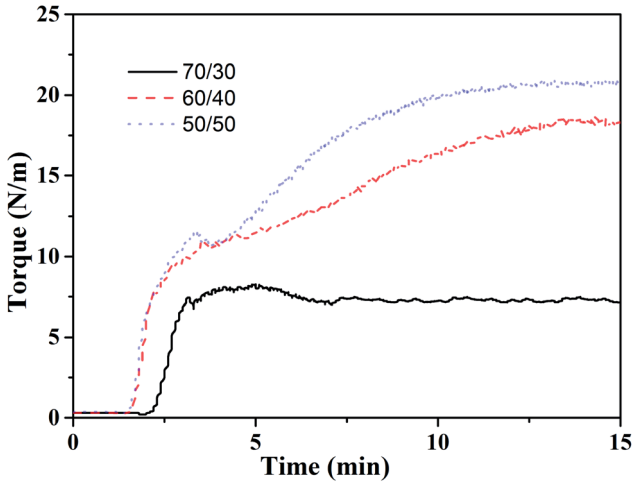

Fig. 3 The dynamic vulcanization curves of SeRM/PLA TPVs with different blending ratios of SeRM/PLA (70/30, 60/40, and 50/50).

observed torque curves of SeRM/PLA TPV system is similar to that of other TPV materials, such as BPE/PLA blends,[22] EPDM/PP TPV,[8,35] NBR/PP TPV,[36] *etc.*

In order to confirm the crosslinking reactions between SeRM molecules and PLA chains, FTIR test of SeRM/PLA (70/30) TPV sample is performed, and the spectrum is given by Fig. 4. For comparison, the FTIR spectra of pure PLA and pure SeRM are also displayed. As indicated by the asterisks (*) in Fig. 4, the peaks located at 1528 cm^{-1} and 1610 cm^{-1} correspond to the characteristic vibrational absorption peaks of carbamate group;[37] these two peaks are observed in FTIP spectrum of SeRM/PLA TPV, yet not present in PLA's or SeRM's. Such a behavior manifests the TDI molecule-induced crosslinking reactions between SeRM and PLA during the dynamic vulcanization.

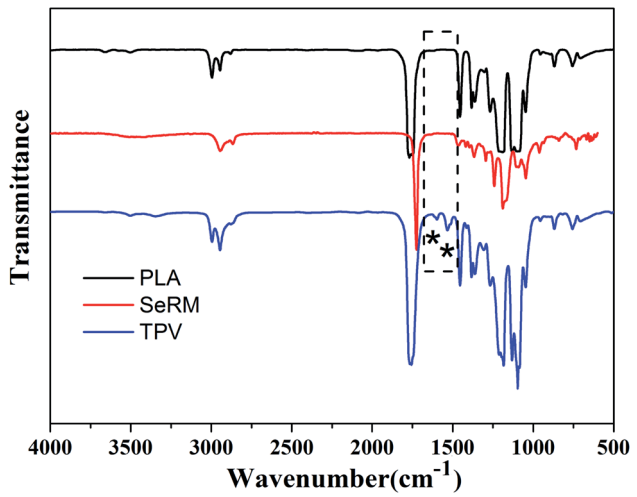

Fig. 4 FTIR spectra of pure PLA, pure SeRM, and SeRM/PLA TPV (70 : 30). Peaks marked with asterisks (*) locate at 1528 cm^{-1} and 1610 cm^{-1}.

3.2 Morphology

Of crucial importance to the overall performance is the TPV morphology, which depends primarily upon the intrinsic properties of rubber and plastic components, the interactions between them, and the processing conditions, *etc.* Here, we shall discuss the TPV morphology affected by blending ratio of rubber to plastic, SeRM to PLA in our case, one of the most critical factors in the formation of TPVs. In principal, the high elasticity of TPV materials (comparable to traditional elastomers) is derived from the original rubbery component, and is successfully achieved by the phase inversion during the processing. Which implies is that too less rubber component proportion cannot effectively construct polymer networks with desired elasticity, but excessive use would also lead to the failure of phase inversion and worse yet the large-sized discontinues particles. Actually, the phase inversion in TPV is more determined by the formation and agglomeration of the rubber particles than the deformation and breakup of the crosslinked rubber phase.[38,39]

Fig. 5 shows the TEM micrographs of bio-based TPVs with varying blending ratios. Owing to the staining effect, PLA appears as the light domains and SeRM as the dark ones. At the low SeRM/PLA ratio of 50/50, the composite seems to exhibit a co-continuous morphology. With increasing the SeRM proportion, the crosslinked SeRM phase is fractured under dynamic shear into large strip-shaped pieces (for 60/40 in Fig. 5b) and even smaller particles (for 70/30 in Fig. 5c) in PLA continuous phase, demonstrating the phase inversion of SeRM/PLA TPV. Specifically, at the blending ratio of 70/30, the SeRM particles appear irregular oval shapes in a stretched behavior, with the size ranging from 1 to 4 μm. However, when the SeRM proportion reaches to too high as 80 wt% (80/20), the SeRM particles would be assembled into large agglomerates of elongated shape, as evidenced by Fig. 5d. Such a aggregation behavior is definitely not conducive to developing phase inversion. By the way, the volume fraction of SeRM particles at 80/20

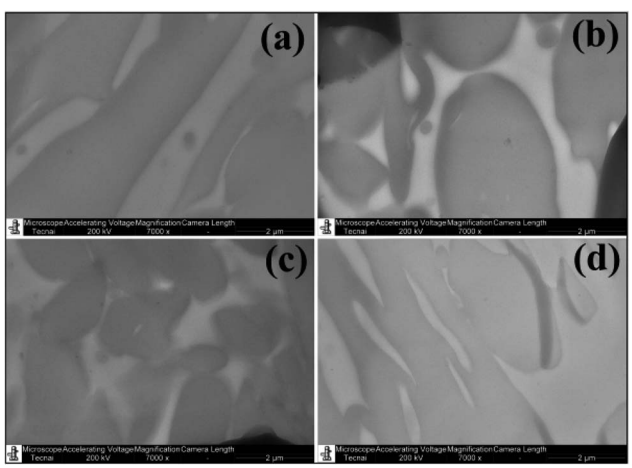

Fig. 5 TEM micrographs of bio-based SeRM/PLA TPVs: (SeRM/PLA, w/w, (a) 50/50; (b) 60/40; (c) 70/30; (d) 80/20). PLA appears as the light domains and SeRM as the dark domains.

blending ratio exceeds the critical percolation threshold of hexagonal close packing (vol% ~74%), probably leading to a bi-continuous phase. It can thus be concluded that a optimal morphology for SeRM/PLA TPVs is obtained at a moderate rubber-plastic blending ratio of 70/30 for our SeRM/PLA TPVs. The schematic illustration of phase inversion at different SeRM/PLA blending ratios is given in Fig. 6 for ease of understanding the TPV morphology.

3.3 Thermal properties

Now we turn our focus to the thermal behavior of bio-based SeRM/PLA TPVs. Fig. 7 shows the DSC curves for a set of SeRM/PLA samples. According to Fig. 7a, pure SeRM has a clear glass transition (T_g) around −45 °C, manifesting flexible chain characteristics and elastomeric behavior, and a distinct melt heat peak (T_m) at 34 °C, demonstrating crystallization behavior. As for the SeRM/PLA blends, all curves (Fig. 7b) exhibit two melting adsorption peaks, a higher one at ~155 °C corresponding to PLA and a lower one at ~34 °C to SeRM. Such a thermal behavior reveals that SeRM/PLA blend is a phase-separated system, in which the two immiscible components keep their own properties. The glass transition of PLA during cooling is clearly observed around 57 °C. However, the glass transition of SeRM becomes elusive compared to pure SeRM. This phenomena may be explained by the suppression in SeRM chain dynamics by the crystallization of PLA and relatively less (compared to pure SeRM) free volume of PLA chains; the minimal thermal effect of SeRM glass transition compared to others such as PLA glass transition and crystallization, can be considered as another possible reason. In addition, the T_g of PLA is seen to shift somewhat towards lower temperatures, indicating a little compatibility between PLA and SeRM, which is originated from the crosslinkages between SeRM and PLA (see the Section of Dynamic Vulcanization).

The heat of cold crystallization of PLA ($T_c \approx 120$ °C) is found to be slightly increased with the addition of SeRM, suggesting a development in cold crystallization of PLA. Understandably, the more flexible (relative to PLA) SeRM molecules introduce more free volume to the composite, and hence the segment mobility of PLA chains is increased, leading to the enhancement of cold crystalline ability of PLA. The slight decrease in T_g of PLA can also be ascribed to the improvement of PLA segment dynamics induced by SeRM molecules.[23]

3.4 Bio-compatibility

For potential applications in biomedical aspects, we need to investigate the bio-compatibility of SeRM/PLA TPV by adopting an *in vitro* cytotoxicity method with MTT colorimetry, as described in the Section of Characterization above. The number of survived cells in the extract using SeRM/PLA TPVs and the relative growth rate (RGR) can be accessed from the value of optical density. Depending on the RGR value, the cytotoxicity of

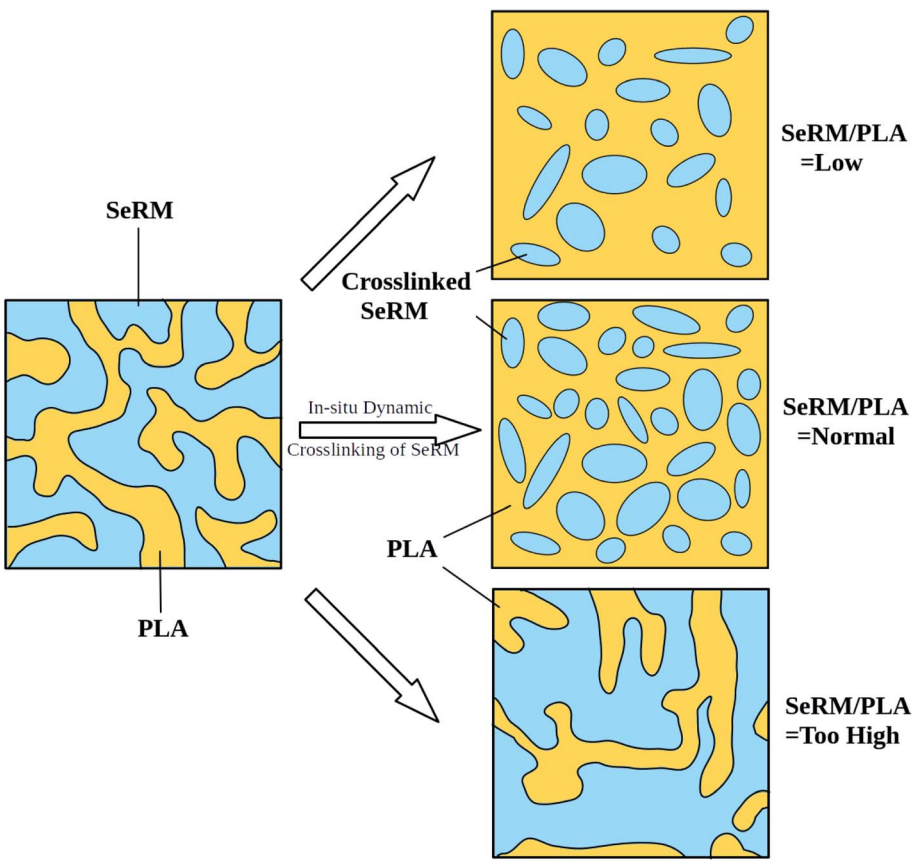

Fig. 6 Schematic illustration of phase inversion with different blending ratios of SeRM/PLA TPVs.

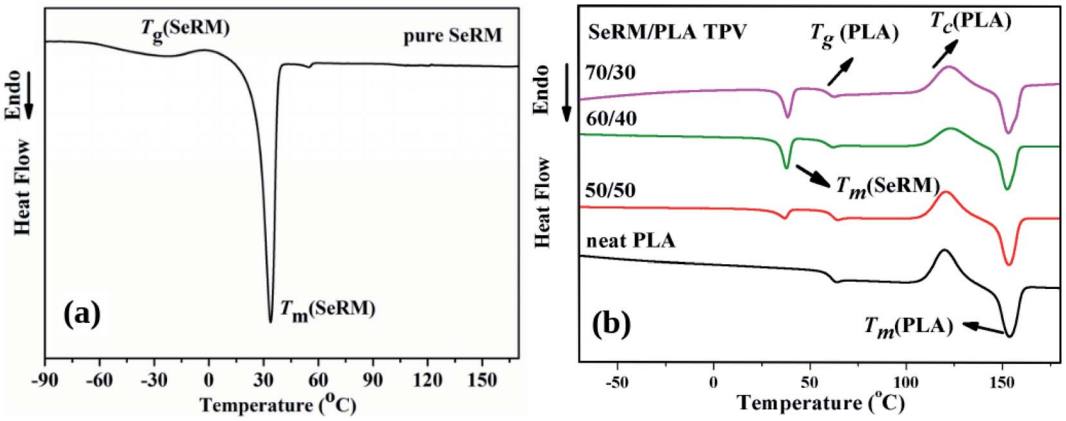

Fig. 7 DSC traces of (a) pure SeRM, and (b) bio-based TPVs with different blending ratios of SeRM/PLA.

materials is classified into six grades, from 0 to 5, corresponding to the cytotoxicity to L929 cells from very low or none to very high, as shown in Table 2. Typically, materials with a grade below 2 could be adequately used for bio-materials. Fig. 8 shows the RGR values of bio-based SeRM/PLA TPVs. All TPV samples are identified to be non-biotoxic to L929 cells, as their RGRs are all above the level of 85% within 3 days. In other words, the cytotoxicity of SeRM/PLA TPVs is Grade 1, exhibiting good biocompatibility. Moreover, the incorporation of SeRM would slightly reduce the cytotoxicity of materials, and the cytotoxicity is seen to decrease with the incubation time of cells.

3.5 Mechanical properties

We here investigate the mechanical properties of TPVs in terms of tensile stress–strain behavior. Fig. 9 shows the stress–strain curves of TPVs with different SeRM/PLA blending ratios, and some representative data are summarized in Table 3. Contrary to the elastomeric mechanical behavior of neat SeRM (Fig. S1†), neat PLA has very high tensile strength but very low elongation at break, a defining characteristic of brittle materials. On the stress–strain curves of SeRM/PLA TPVs, however, the plastic feature with necking and yielding is no more observed and the elongation at break is much improved; they behave like typical elastomers. Strictly speaking, the 50/50 SeRM/PLA blend cannot be considered as a good TPV in that a quasi-yielding occurs at the strain of ~10%. By increasing the SeRM content from 60/40 to 80/20 (w/w), the SeRM/PLA TPVs develop into more elastic and soft materials, as evidenced by the reduction in tensile strength from ~14 MPa to ~4.0 MPa and the decrease in hardness from 90° to 76°. The underlying mechanism behind such a mechanical behavior of SeRM/PLA TPVs lies in the unique sliding effect of SeRM molecules when subjected to deformations. It should be noticed that the elongation at break of TPV with a blending ratio of 80/20 is relatively low, presumably due to the nonuniform distribution and the agglomeration of crosslinked SeRM particles in PLA matrix.

Furthermore, molecular dynamics simulations are implemented to testify the sliding effect of α-CD molecules along the PEG axial chain. Fig. 10 shows some representative SeRM molecules under uniaxial tensile deformation. For ease of directly monitoring, only two representative SeRM molecules, each carrying three α-CD rings, are shown in VMD snapshots, and arrows are applied to indicate the relative movement of α-CD molecules and PEG chains. For uncrosslinked SeRM/PLA TPV system (Fig. 10a), there are no observable relative displacement between α-CD rings and PEG axial chain during the deformations, *viz.*, none sliding effect. On the contrary, α-CD rings in crosslinked SeRM/PLA TPV system are clearly seen to slide along the PEG axial, exhibiting significant sliding effect, as shown in Fig. 10b. The interesting sliding effect is intrinsically induced by the drag force on side PCL chains from other SeRM molecules or PLA chains with chemical bonding (crosslinkages) under deformations. In another word, the

Table 2 Cytotoxicity grade with respect to relative growth rate (RGR)

Cytotoxicity grade	0	1	2	3	4	5
RGR (%)	≥100	75–99	50–74	25–49	1–24	0

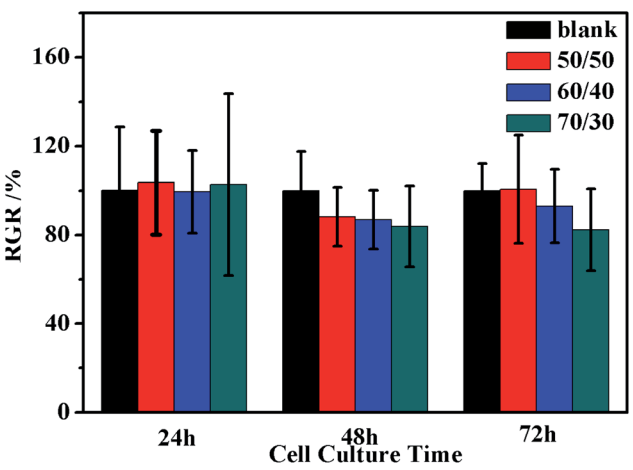

Fig. 8 RGR value of bio-based SeRM/PLA TPVs as a function of incubation time.

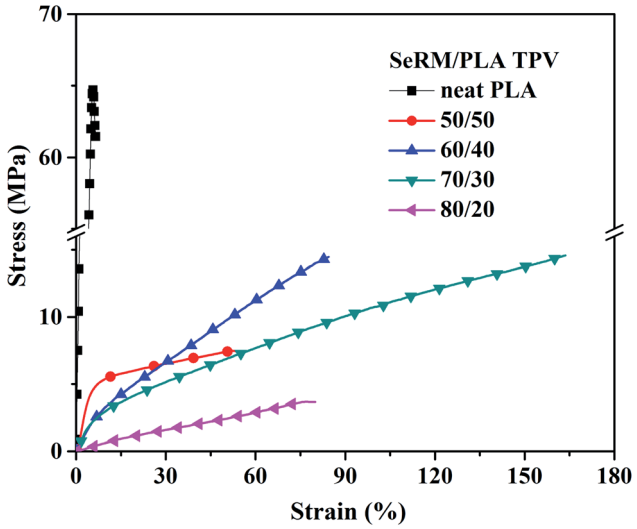

Fig. 9 Stress–strain curves of TPVs with different blending ratios of SeRM to PLA.

Table 3 Mechanical properties of SeRM/PLA TPVs

SeRM/PLA (w/w)	Tensile strength (MPa)	Elongation at break (%)	Shore A hardness (°)
0/100	64.1 ± 2.5	5 ± 1	—
50/50	7.7 ± 4.4	55 ± 3	97
60/40	14.1 ± 5.4	88 ± 5	90
70/30	14.7 ± 5.8	164 ± 6	85
80/20	4.0 ± 2.5	78 ± 5	76

crosslinking endows considerable elasticity to the SeRM phase. In addition, the major differences in the response to external stress between flexible elastomers and rigid thermoplastics, especially in case of unfavorable interface compatibility, would usually lead to extensive stress concentration and undesirable deterioration in mechanical properties; however, in this crosslinked SeRM/PLA case such an imbalance can be reduced by the stress distribution by sliding effect and better load transfer enhanced by chemical bonding between PCL and PLA. In general, the sliding effect of SeRM molecules can significantly improve the overall mechanical properties of SeRM/PLA TPV materials.

4 Conclusion

The present work reported a novel bio-based thermoplastic vulcanizate (TPV) through reactive blending of polylactide (PLA) and slide ring polymer material (SeRM). The properties of SeRM/PLA TPVs were systematically investigated by both experimental tools and molecular dynamics simulations. Phase inversion of SeRM/PLA blends was observed during the dynamic vulcanization, and an optimum phase inversion state was obtained at the blending ratio of 70/30 w/w. In TEM images, the majority of SeRM particle that were dispersed in PLA continuous phase were found to have an average diameter of 1 ~4 μm. Thermal analysis by DSC confirmed the phase separation between the rubber component of SeRM and the thermoplastic component of PLA. Glass transition temperature of PLA was slightly decreased, owing to the improvement in interface compatibility by chemically bonding the PCL side chains (of SeRM molecules) and PLA chains. Besides, cytotoxicity method

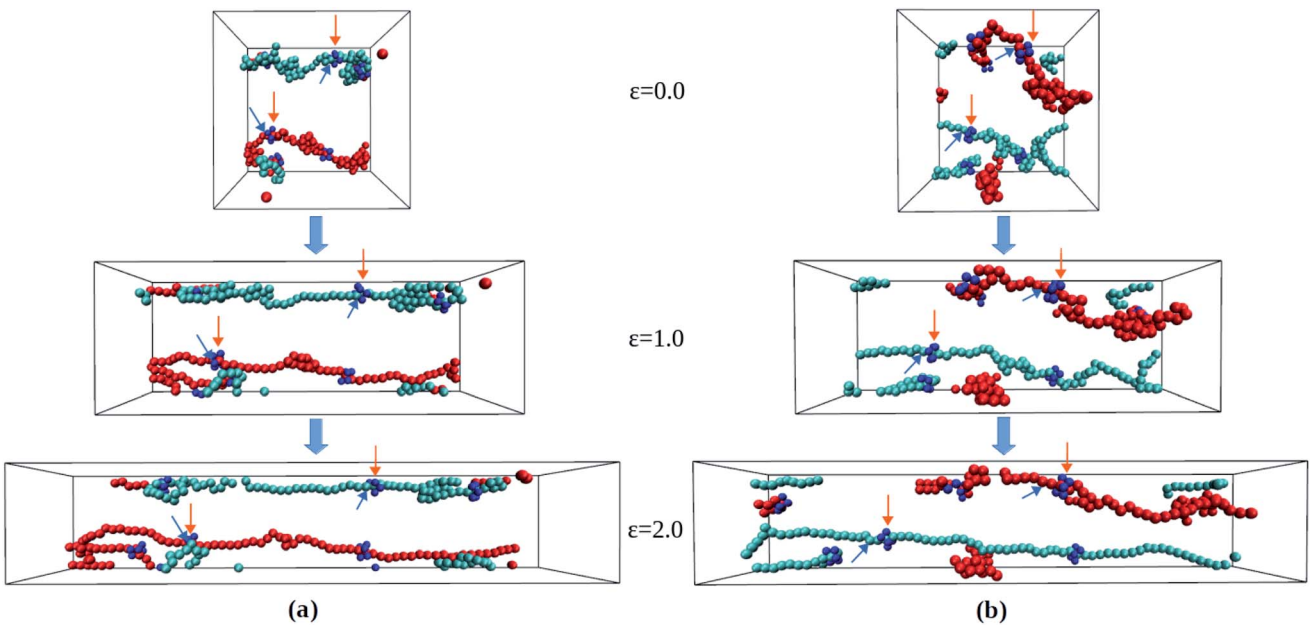

Fig. 10 VMD snapshots of (a) uncrosslinked and (b) crosslinked SeRM/PLA TPVs under uniaxial tensile deformation. For clear observations, only two representative SeRM molecules are shown in each simulation system. The blue spheres represent α-CD molecule, and the ones with red and cyan colors denote the PEG chains in different SeRM molecules. The red and blue arrows point to the examined α-CD molecule and a close PEG bead.

with MTT colorimetry indicated that the bio-based TPVs had no cytotoxicity to L929 cells. The tensile strength and elongation at break of TPVs were approximately 14.7 MPa and 164%, respectively, at the SeRM/PLA blending ratio of 70/30. The significant improvement in mechanical properties of SeRM/PLA TPVs would be ascribed to the unique sliding effect of SeRM molecules when subjected to deformations. In general, the SeRM/PLA TPVs is believed to have potential applications in both biomedical and engineering fields.

Conflicts of interest

There are no conflicts to declare.

Acknowledgements

This work is supported by the Natural Science Foundation of Zhejiang Province, China (LY22B040002, LQ19E030013), the Science and Technology Research Projects of Jiaxing City, Zhejiang Province (2019AD32007, 2020AY10004), and Key Research Projects in Jiaxing Nanhu University (N41472001-49).

Notes and references

1 N. Ning, S. Li, H. Wu, H. Tian, P. Yao, H. Guo-Hua, M. Tian and L. Zhang, *Prog. Polym. Sci.*, 2018, **79**, 61–97.
2 S. Salaeh, A. Das, K. W. Stoeckelhuber and S. Wiessner, *Composites, Part A*, 2020, **130**, 105763.
3 R. Cui, J. Ding and Y. Chen, *Composites, Part A*, 2019, **122**, 27–35.
4 R. J. Spontak and N. P. Patel, *Curr. Opin. Colloid Interface Sci.*, 2000, **5**, 333–340.
5 J. K. Mishra, G.-H. Kim, I. Kim, I.-J. Chung and C.-S. Ha, *J. Polym. Sci., Part B: Polym. Phys.*, 2004, **42**, 2900–2908.
6 S. S. Banerjee and A. K. Bhowmick, *J. Mater. Sci.*, 2016, **51**, 6722–6734.
7 R. R. Babu and K. Naskar, *Advanced Rubber Composites*, 2010, pp. 219–247.
8 H. Wu, M. Tian, L. Zhang, H. Tian, Y. Wu and N. Ning, *Soft Matter*, 2014, **10**, 1816–1822.
9 Q. Wu, J. Fang, M. Zheng, Y. Luo, X. Wang, L. Xu and C. Zhang, *Polymers*, 2019, **11**, 175.
10 V. Litvinov, *Macromolecules*, 2006, **39**, 8727–8741.
11 H. Kang, M. Gong, M. Xu, H. Wang, Y. Li, Q. Fang and L. Zhang, *Ind. Eng. Chem. Res.*, 2019, **58**, 6375–6384.
12 P. Yao, H. Wu, N. Ning, L. Zhang, H. Tian, Y. Wu, G.-H. Hu, T. W. Chan and M. Tian, *RSC Adv.*, 2016, **6**, 30004–30013.
13 D. K. Schneiderman and M. A. Hillmyer, *Macromolecules*, 2017, **50**, 3733–3749.
14 H. Kang, B. Qiao, R. Wang, Z. Wang, L. Zhang, J. Ma and P. Coates, *Polymer*, 2013, **54**, 2450–2458.
15 K. Hasheminejad and A. Montazeri, *Appl. Surf. Sci.*, 2020, **502**, 144150.
16 A. P. Mathew, K. Oksman and M. Sain, *J. Appl. Polym. Sci.*, 2005, **97**, 2014–2025.
17 Y. Gao, Y. Li, X. Hu, W. Wu, Z. Wang, R. Wang and L. Zhang, *Polymers*, 2017, **9**, 694.
18 Z. Gong, J. Huang, J. Fan, X. Chen, H. Wang and Y. Chen, *Ind. Eng. Chem. Res.*, 2022, **61**(1), 359–371.
19 M. Bednarek, K. Borska and P. Kubisa, *Polym. Rev.*, 2021, **61**, 493–519.
20 C. Bueno-Ferrer, E. Hablot, F. Perrin-Sarazin, M. C. Garrigós, A. Jiménez and L. Averous, *Macromol. Mater. Eng.*, 2012, **297**, 777–784.
21 G.-C. Liu, Y.-S. He, J.-B. Zeng, Q.-T. Li and Y.-Z. Wang, *Biomacromolecules*, 2014, **15**, 4260–4271.
22 H. Kang, X. Hu, M. Li, L. Zhang, Y. Wu, N. Ning and M. Tian, *RSC Adv.*, 2015, **5**, 23498–23507.
23 X. Li, H. Kang, J. Shen, L. Zhang, T. Nishi, K. Ito, C. Zhao and P. Coates, *Polymer*, 2014, **55**, 4313–4323.
24 K. Ito, *Curr. Opin. Solid State Mater. Sci.*, 2010, **14**, 28–34.
25 J. Araki, T. Kataoka and K. Ito, *Soft Matter*, 2008, **4**, 245–249.
26 T. Sakai, H. Murayama, S. Nagano, Y. Takeoka, M. Kidowaki, K. Ito and T. Seki, *Adv. Mater.*, 2007, **19**, 2023–2025.
27 L. Jiang, C. Liu, K. Mayumi, K. Kato, H. Yokoyama and K. Ito, *Chem. Mater.*, 2018, **30**, 5013–5019.
28 J. S. Trent, J. I. Scheinbeim and P. R. Couchman, *Macromolecules*, 1983, **16**, 589–598.
29 K. Kremer and G. S. Grest, *J. Chem. Phys.*, 1990, **92**, 5057–5086.
30 Z. Zhang, G. Hou, J. Shen, J. Liu, Y. Gao, X. Zhao and L. Zhang, *Polymers*, 2018, **10**, 964.
31 S. Plimpton, *J. Comput. Phys.*, 1995, **117**, 1–19.
32 J. Shen, X. Lin, J. Liu and X. Li, *Macromolecules*, 2018, **52**, 121–134.
33 J. Shen, X. Lin, J. Liu and X. Li, *Phys. Chem. Chem. Phys.*, 2020, **22**, 16760–16771.
34 X. Li, H. Kang and J. Shen, *Polymer*, 2020, **211**, 123077.
35 C. F. Antunes, A. Machado and M. Van Duin, *Eur. Polym. J.*, 2011, **47**, 1447–1459.
36 J. Oderkerk and G. Groeninckx, *Polymer*, 2002, **43**, 2219–2228.
37 K. B. H. Badri, W. C. Sien, M. Shahrom, L. C. Hao, N. Y. Baderuliksan, N. Norzali, *et al.*, *Solid State Sci. Technol.*, 2010, **18**, 1–8.
38 H. Wu, M. Tian, L. Zhang, H. Tian, Y. Wu, N. Ning and T. W. Chan, *ACS Sustainable Chem. Eng.*, 2015, **3**, 26–32.
39 S. Krishnan, S. Mohanty and S. K. Nayak, *J. Macromol. Sci., Part A: Pure Appl.Chem.*, 2017, **54**, 547–555.